

Chapter 14

Fluorescence Lifetime Measurements of NAD(P)H in Live Cells and Tissue

Alex J. Walsh, Amy T. Shah, Joe T. Sharick
and Melissa C. Skala

Abstract Autofluorescence intensity and lifetime imaging of NAD(P)H yields quantitative, non-invasive measurements of cellular metabolism. NAD(P)H is a coenzyme involved in cellular metabolism processes including glycolysis and oxidative phosphorylation. The NAD(P)H fluorescence lifetime includes a short and long lifetime component due to the two possible physiological conditions of NAD(P)H, free or protein-bound (to an enzyme and/or substrate). Fluorescence lifetimes of NAD(P)H have been imaged in cells, ex vivo tissues, and in vivo tissues to investigate cellular metabolism at basal conditions and with perturbations. In particular, NAD(P)H fluorescence lifetimes are altered in pre-malignant and malignant cells and tissues compared with non-malignant cells and tissues across several cancers including head and neck cancers, breast cancer, and skin cancer. Additionally, NAD(P)H fluorescence lifetimes decrease in cancer cells and tumors following drug treatment and therefore, these metabolic endpoints show potential for drug monitoring and screening.

14.1 Introduction

The reduced form of nicotinamide adenine dinucleotide (NAD(P)H) is a co-enzyme in cellular metabolism. It functions as the main electron donor in oxidative phosphorylation, and also in the reactions that feed into oxidative phosphorylation (e.g.

A.J. Walsh · A.T. Shah · J.T. Sharick · M.C. Skala (✉)
Department of Biomedical Engineering, Vanderbilt University,
Nashville, TN 37235, USA
e-mail: m.skala@vanderbilt.edu

A.J. Walsh
e-mail: alexandra.j.walsh@vanderbilt.edu

A.T. Shah
e-mail: a.shah@vanderbilt.edu

J.T. Sharick
e-mail: joseph.t.sharick@vanderbilt.edu

glycolysis, citric acid cycle, etc.). NAD(P)H is autofluorescent, with an excitation maximum at 350 nm and an emission maximum at 460 nm [46]. Intracellular NAD(P)H is localized in the cytoplasm and mitochondria. Early optical imaging studies focused on mapping NAD(P)H intensities in cells and tissues, in order to gain non-invasive insight into relative cellular metabolic rates [11]. The fluorescence lifetime of NAD(P)H provides further information on the relative amounts of free and protein-bound NAD(P)H [40]. The fluorescence lifetime of free NAD(P)H (~ 300 ps) is distinctly different from that of protein-bound NAD(P)H (~ 2.5 ns) due to quenching from the adenine moiety of the molecule when it is in its free state.

The fluorescence decay function of NAD(P)H is an advantageous measure compared with fluorescence intensity because the lifetime provides additional information on protein-binding activity whereas the NAD(P)H fluorescence intensity spectrum is similar for both the free and protein-bound conformations. Additionally, the decay parameters are independent of concentration and are therefore a self-referenced measure which require less system calibration compared with intensity measurements. The fluorescence lifetimes and the relative amounts of bound and unbound NAD(P)H have been characterized in cell culture, applied to animal models to understand disease progression, and piloted in human tissues both *ex vivo* and *in vivo*. These studies have provided unique insight into the role of cellular metabolism in pathology and in response to therapy. Future technology development will exploit the fluorescence lifetime of NAD(P)H to streamline disease diagnosis, improve treatment monitoring, and accelerate meaningful drug development.

14.2 NAD(P)H Fluorescence Lifetime in Cells

The fluorescence decay of NAD(P)H is typically fit by a double-exponential decay model, where the short component represents free NAD(P)H and the long component represents protein-bound NAD(P)H. The amplitude-weighted (mean) lifetime is calculated by $\tau_m = \alpha_1\tau_1 + \alpha_2\tau_2$, where α_1 and α_2 represent the relative contributions from free and protein-bound NAD(P)H, respectively ($\alpha_1 + \alpha_2 = 1$), and τ_1 and τ_2 represent the lifetimes of the free and protein-bound components, respectively. In order to record the fast lifetime component correctly the time-channel width should be no larger than about 1/5 of its decay time. The number of time channels should be large enough to cover a time interval of about 5 times the slow decay component [34]. That means the time channel width should be about 50 ps, and the number of time channels about 250. These numbers are in the range where TCSPC delivers near-ideal photon efficiency [4]. Moreover, correct double-exponential decay components are only obtained if the data are free of out-of-focus fluorescence. Therefore, an imaging technique with optical sectioning capability must be used. These requirements are almost perfectly met by TCSPC FLIM in combination with confocal or multiphoton laser scanning, see Chap. 2. Most of the data shown in this section were recorded by TCSPC FLIM in combination with two-photon laser scanning microscopes. Our own system uses a Becker & Hickl

SPC-150 TCSPC FLIM module [6] with a Hamamatsu H7422P-40 PMT in combination with a Prairie Technology two-photon laser scanning microscope.

The fluorescence lifetime of cellular NAD(P)H has been characterized for several metabolic perturbations, including treatment with metabolic inhibitors. The NAD(P)H lifetime has also been characterized for cancer cells expressing particular mutations and in response to anti-cancer treatment. Additionally, the NAD(P)H lifetime has been investigated to differentiate mechanisms of cell death and to measure stem cell differentiation.

Metabolic perturbations have been shown to affect the fluorescence lifetime of NAD(P)H, see also Chap. 13. In particular, these perturbations include adding inhibitors of oxidative phosphorylation or glycolysis. The electron transport chain is a series of oxidation and reduction reactions that create a proton gradient across the mitochondrial membrane, and this gradient drives ATP synthesis. During the electron transport chain, NAD(P)H is oxidized to NAD⁺, but this oxidation can be disrupted by compounds like cyanide. Cyanide treatment causes a decrease in the mean NAD(P)H lifetime (τ_m) in cell lines from the breast (MCF10A) and oral cavity (OKF6) [8, 55, 60]. This decrease in τ_m reflects an increase in the contribution from free NAD(P)H (α_1).

Oxidative phosphorylation inhibition achieved with cobalt chloride (CoCl₂) treatment in MCF10A cells (Fig. 14.1) and with rotenone treatment in BKEz-7 endothelial cells from calf aorta cause similar shifts in NAD(P)H τ_m and α_1 [51]. Inhibition of glycolysis in MCF10A cells caused an increase in the NAD(P)H protein-bound lifetime (τ_2) and a decrease in the relative amount of protein-bound NAD(P)H (α_2) (Fig. 14.1). Glycolysis inhibition with deoxyglucose treatment in the BKEz-7 cells caused a slight increase in NAD(P)H τ_m , reflecting an increase in NAD(P)H α_2 , but statistical significance was not tested [51].

In addition to metabolic inhibitors, serum starvation and cellular confluency affect cellular metabolism and induce changes in the NAD(P)H lifetime. Serum levels in media can affect cellular metabolism because serum contains substrates that are used in glycolysis and oxidative phosphorylation. Serum-starvation in MCF10A cells causes increased NAD(P)H α_1 and decreased NAD(P)H τ_m , which are similar effects as those observed due to treatment with cyanide [8]. Serum-starvation and oxidative phosphorylation inhibition affect the NAD(P)H lifetime

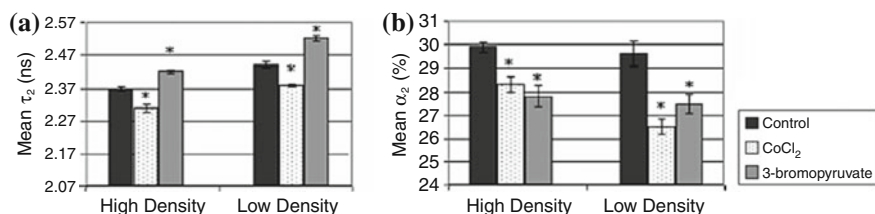


Fig. 14.1 The long-lifetime component of NAD(P)H decreases with CoCl₂ treatment and increases with 3-bromopyruvate treatment in high-density and low-density MCF10A cells (a). The contribution from the long-lifetime component decreases with CoCl₂ and 3-bromopyruvate treatment in MCF10A cells (b). Reproduced with permission from [56]

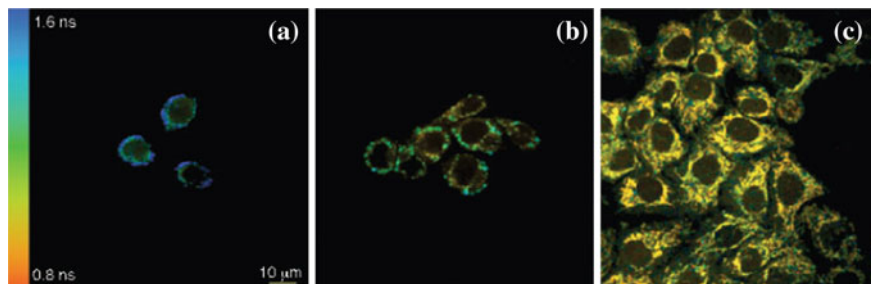


Fig. 14.2 Representative images show MCF10A cells at a higher confluency have a lower NAD(P)H fluorescence lifetime. Reproduced with permission from [8]

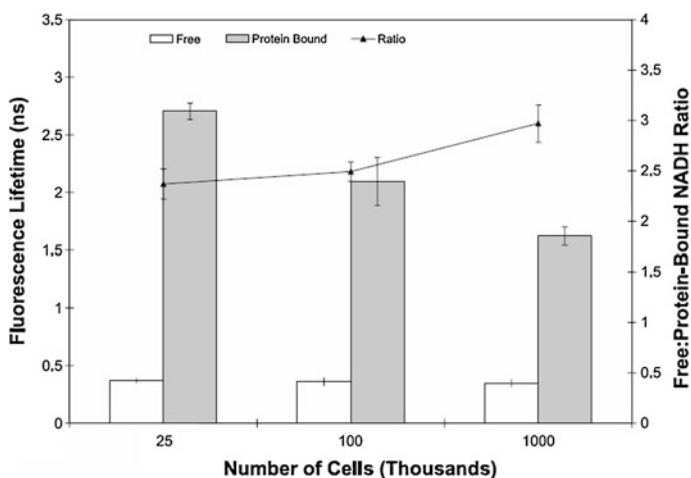


Fig. 14.3 MCF10A cells that have been serum-starved show increased free-to-protein-bound NAD(P)H ratio plated at 10,000 cells per dish compared with at 25 and 100 cells per dish. Reproduced with permission from [8]

similarly since both perturbations slow cellular metabolism. Confluency also affects cellular metabolism. A higher confluency increases NAD(P)H α_1 and decreases NAD(P)H τ_2 , causing a decreased NAD(P)H τ_m , see Figs. 14.2 and 14.3.

The fluorescence lifetime of NAD(P)H has been shown to distinguish malignant versus non-malignant cells and as well as different sub-types of malignant cells based on receptor status. Common phenotypes in breast cancers include overexpression of the estrogen receptor (ER) and human epidermal growth factor receptor 2 (HER2). Walsh et al. measured the NAD(P)H fluorescence lifetime of malignant breast cancer cells including MCF7, which express ER, as well as SKBr3, MDA-MB-361, and BT474, which express HER2 (Fig. 14.4). The NAD(P)H lifetime of malignant cells was greater than that of the non-malignant cell line MCF10A [60]. This increase was attributed to a decreased NAD(P)H α_1 . Furthermore, the NAD(P)H mean lifetime of

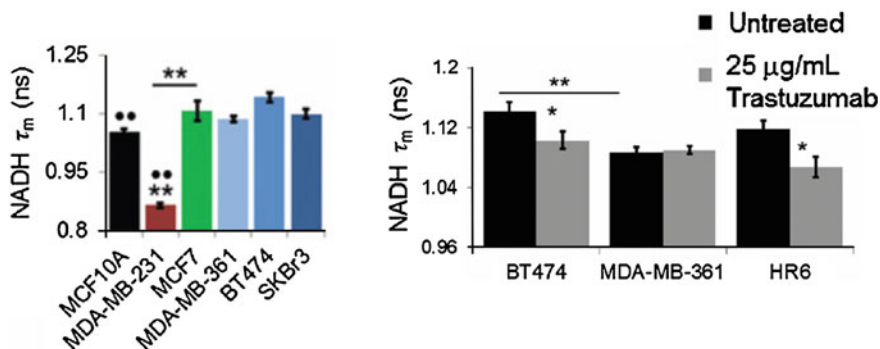


Fig. 14.4 *Left* NAD(P)H lifetime is decreased in triple negative breast cancer (MDA-MB-231) compared to non-malignant breast cells (MCF10A) and increased in estrogen receptor positive (MCF7) and HER2 positive cells (MDA-MB-361, BT474, SKBr3). *Right* NAD(P)H lifetime decreases in BT474 cells with trastuzumab treatment, is unchanged in MDA-MB-361 cells, and is decreased in HR6 cells with trastuzumab treatment. Reproduced with permission from [60]

the MDA-MB-231 breast cancer cells, which do not overexpress ER or HER2, was lower than that of the MCF10A cells. Additionally, squamous cell carcinoma cells from the oral cavity, including SCC25 and SCC61, show an increased NAD(P)H α_1 compared with the nonmalignant cell line OKF6 [55].

Walsh et al. showed that the NAD(P)H lifetime can resolve response to anti-cancer treatment. These studies were tested in breast cancer cells with treatment using trastuzumab, which is a clinically-used antibody that targets HER2 and prevents downstream signalling. The cell lines studied included a trastuzumab-responsive cell line, BT474, and a partly responsive cell line, MDA-MB-361. Additionally, a cell line derived from a BT474 xenograft with an acquired resistance to trastuzumab, HR6, was also measured. Trastuzumab treatment for 24 h caused a decrease in the mean NAD(P)H lifetime in BT474, but not MDA-MB-361 cells (Fig. 14.4). This change in NAD(P)H lifetime in BT474 cells was attributed to an increased contribution from free NAD(P)H. Interestingly, the HR6 cells also showed a decreased mean NAD(P)H lifetime, which could reflect altered internal signalling from trastuzumab treatment.

Shah et al. tested therapeutic response in oral cancer cells treated with cetuximab, an antibody that targets the epidermal growth factor receptor (EGFR), BGT226, an investigational small molecular inhibitor that targets phosphoinositide 3-kinase (PI3K) and mammalian target of rapamycin (mTOR), and cisplatin, standard chemotherapy. Treatment with these drugs for 24 h was done in SCC25 and SCC61, two EGFR-overexpressing cell lines (Figs. 14.5 and 14.6). SCC61 cells also have upregulated PI3K activation. For both cell lines, the contribution of free NAD(P)H was shown to decrease with BGT226 and cisplatin treatment (Fig. 14.6). However, SCC61 cells also show a decreased contribution from free NAD(P)H with cetuximab treatment, which could reflect altered metabolic pathways in response to treatment. These results indicate that the NAD(P)H decay parameters are a sensitive measure that can resolve early response to anti-cancer treatment.

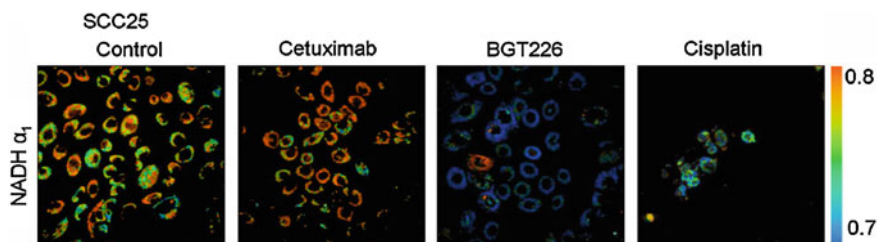


Fig. 14.5 Representative images show NAD(P)H α_1 of SCC25 cells after treatment with cetuximab, BGT226, or cisplatin for 24 h. Reproduced with permission from [55]

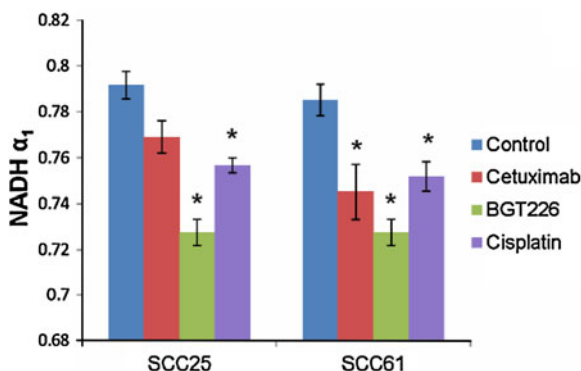


Fig. 14.6 NAD(P)H α_1 decreases with BGT226 and cisplatin treatment in SCC25 and SCC61 cells after 24 h of treatment. Additionally, NAD(P)H α_1 decreases with cetuximab treatment in SCC61 cells. Reproduced with permission from [55]

The NAD(P)H fluorescence lifetime has been used to characterize cell death by apoptosis or necrosis [61]. Wang et al. treated HeLa cells and 143 osteosarcoma cells with staurosporine (STS) to induce apoptosis or hydrogen peroxide (H_2O_2) to induce necrosis. STS treatment caused an initial increase in NAD(P)H lifetime 15 min after treatment and then a gradual decrease for up to two hours (Fig. 14.7). These effects are attributed to an increased contribution of protein-bound NAD(P)H or an increased lifetime of protein-bound NAD(P)H, reflecting NAD(P)H binding to different enzymes in apoptosis. Necrosis caused no change in NAD(P)H fluorescence lifetime over one hour (Fig. 14.8). To validate the process of apoptosis, STS treatment showed increased caspase 3 activity compared with H_2O_2 treatment after two hours. These results indicate that the NAD(P)H lifetime has potential to be a label-free method to distinguish methods of cell death, which could provide beneficial information for optimizing treatments that cause apoptosis instead of necrosis.

Stem cell differentiation has been characterized using NAD(P)H fluorescence lifetime [28, 39]. Guo et al. incubated human mesenchymal stem cells (hMSCs) in osteogenic induction media, causing osteogenic differentiation. Over 21 days,

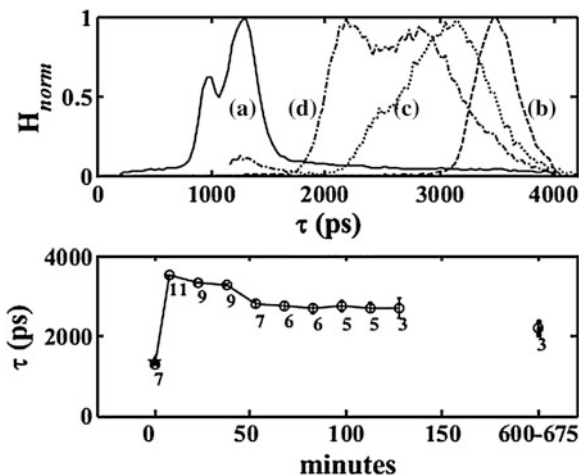


Fig. 14.7 The *top graph* shows distributions of lifetimes from (a) before treatment with STS and after treatment for 0–15 min (b), 30–45 min (c), and 60–75 min (d). The *bottom graph* shows the average lifetime, τ , over time after STS treatment. Reproduced with permission from [61]

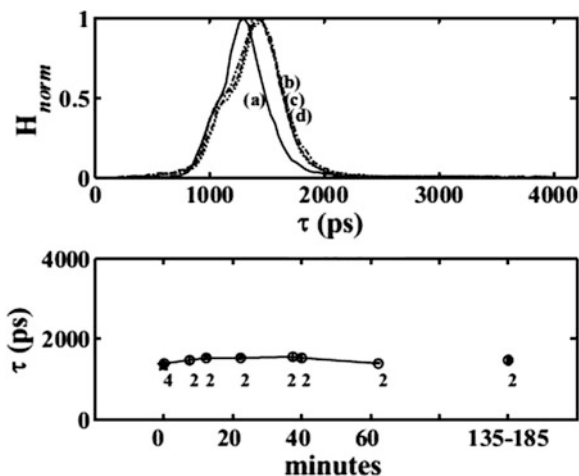


Fig. 14.8 The *top graph* shows distributions of lifetimes from (a) before treatment with H_2O_2 and after treatment for 0–15 min (b), 30–50 min (c), and 50–70 min (d). The *bottom graph* shows the average lifetime, τ , over time after H_2O_2 treatment. Reproduced with permission from [61]

osteogenic differentiation caused an increase in the mean lifetime of NAD(P)H and a decrease in the ratio between free and protein-bound NAD(P)H.

Overall, the fluorescence lifetime of NAD(P)H is a sensitive measure of metabolic processes, particularly for applications for characterizing cancer cells and response to anti-cancer treatment, measure the effect of inhibitors targeting metabolic pathways, characterizing cell death, and monitoring stem cell differentiation.

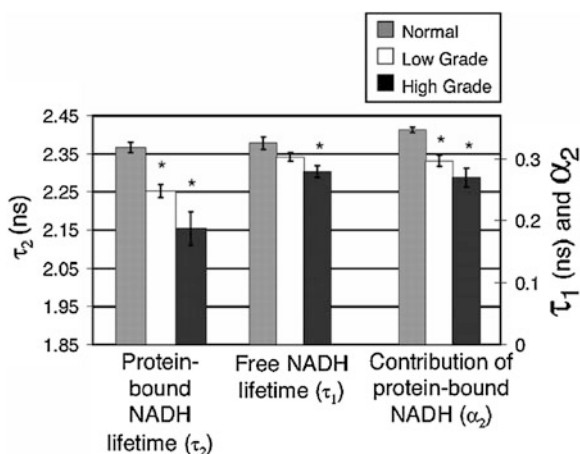
14.3 NAD(P)H Fluorescence Lifetime in Preclinical Models

Preclinical models of human cancers remain a vital step in the drug discovery and development process. Understanding the pathophysiology of cancer, studying the mechanisms of intrinsic and acquired resistance to therapies, and identifying novel therapeutic targets and agents rely on the use of a wide spectrum of animal models [49]. Both transgenic and carcinogen-promoter-induced tumor models will be discussed in this section. The former are similar to human cancers in their phenotype, histology, and genetic makeup, and allow for the development of tumors in their appropriate microenvironment, but may develop asynchronously and are time and labour intensive. The latter are similar to human cancers in their phenotype, histology, and biochemistry, and are highly reproducible, but require repeated applications of carcinogens and require a long time frame for tumor development [49]. While animal models are imperfect representations of genetically heterogeneous human cancers, they are indispensable for the testing of new diagnostic imaging modalities and devices prior to translation to a clinical setting.

The ability of optical metabolic imaging to distinguish precancerous cells from normal cells has been investigated *in vivo* using the hamster cheek pouch model of oral cancer, which mimics the development of squamous epithelial cancer in the human oral cavity [1]. Skala et al. demonstrated the use of multiphoton microscopy to simultaneously image NAD(P)H lifetime and subcellular morphology in this model, which was generated by treatment with 0.5 % DMBA, a powerful carcinogen [57]. A significant decrease in the contribution and lifetime of protein-bound NAD(P)H was reported in epithelial precancers versus normal tissue (Fig. 14.9), along with a significant increase in intracellular variability of NAD(P)H fluorescence lifetimes.

Neoplastic cells, like the ones present in epithelial precancers, favour glycolysis over oxidative phosphorylation as a means of generating ATP [27], which is consistent with the observed decrease in contribution of protein-bound NAD(P)H

Fig. 14.9 Volume-averaged NAD(P)H lifetime variables in normal, low-grade precancerous, and high-grade precancerous animals obtained from *in vivo* multiphoton images. Reproduced with permission from [57]



lifetime in these cells. The decrease in protein-bound NAD(P)H lifetime is attributed to a possible increase in dynamic quenching [41] or a change in distribution of NAD(P)H enzyme binding sites in neoplastic tissues [2]. This study demonstrates an *in vivo* application of multiphoton lifetime imaging for high-resolution metabolic mapping, guiding development of similar time-resolved and steady state fluorescence schemes for clinical detection of human precancers and cancers.

Jabbour et al. has developed a multimodal optical system for imaging of oral precancer that takes advantage of this ability of multiphoton FLIM to probe the metabolic activity in possibly precancerous tissue [30]. The integrated system uses FLIM to generate real-time wide-field images of the biochemical makeup of the specimen, which then guide reflectance confocal microscopy (RCM) imaging to suspicious sites within the field of view (FOV). RCM allows clinicians to probe subcellular morphology and is able to distinguish between normal, precancerous, and cancerous oral tissue [18], but has a limited FOV and thus requires guidance, usually by visual inspection. The multimodal optical system was built using an automated translation stage which moved a sample between the FOVs of two separate FLIM and RCM subsystems. The FOV of the FLIM subsystem was $16 \times 16 \text{ mm}^2$ with a lateral resolution of $62.5 \text{ }\mu\text{m}$, while the RCM subsystem FOV was measured to have a $400 \text{ }\mu\text{m}$ diameter with a lateral resolution of $0.97 \text{ }\mu\text{m}$. In the FLIM subsystem, three emission collection spectral bands were generated, including one corresponding to NAD(P)H ($452 \pm 22.5 \text{ nm}$). The illumination source for the RCM subsystem was a near infrared continuous wave diode-pumped solid state laser with $\lambda = 1064 \text{ nm}$ (power at sample $<45 \text{ mW}$).

The ability of the multimodal optical system to differentiate between normal and precancerous tissue *in vivo* was tested using the same hamster cheek pouch model of oral cancer described above. For imaging, the hamster was anesthetized, and the cheek pouch pulled and clamped to a mount. FLIM imaging was performed first, and spatial features of the FLIM intensity and lifetime images were used to choose locations for RCM (15 per treated pouch) (Fig. 14.10).

As expected, NAD(P)H fluorescence intensity and lifetime is relatively consistent within healthy tissue. The RCM images taken from the centre of the FOV in Fig. 14.10b, c, g shows keratin scattering at the surface, as well as epithelial nuclei beneath the outer layer. FLIM and RCA images from a DMBA-treated hamster cheek pouch show significant variability in fluorescence intensities, lifetimes, and cell morphologies (Fig. 14.11). The NAD(P)H fluorescence lifetime was found to be much shorter ($2.62 \pm 0.79 \text{ ns}$) compared to normal tissue ($4.60 \pm 0.25 \text{ ns}$) and low-grade dysplasia ($4.29 \pm 0.29 \text{ ns}$) (Region 2). This is expected due to an increased fluorescence contribution from bound NAD(P)H. Corresponding RCM images show larger cell nuclei in Region 2 versus Region 1, consistent with the respective diagnoses of low-grade dysplasia and cytologic atypia by histopathology. The classification ability of this dual-modality system could have clinical relevance in assessing whether a sample is normal, benign, premalignant, or malignant.

For situations in which *in vivo* optical measurements are not feasible, it has been shown that FLIM measurements in excised tissue maintained in chilled tissue media

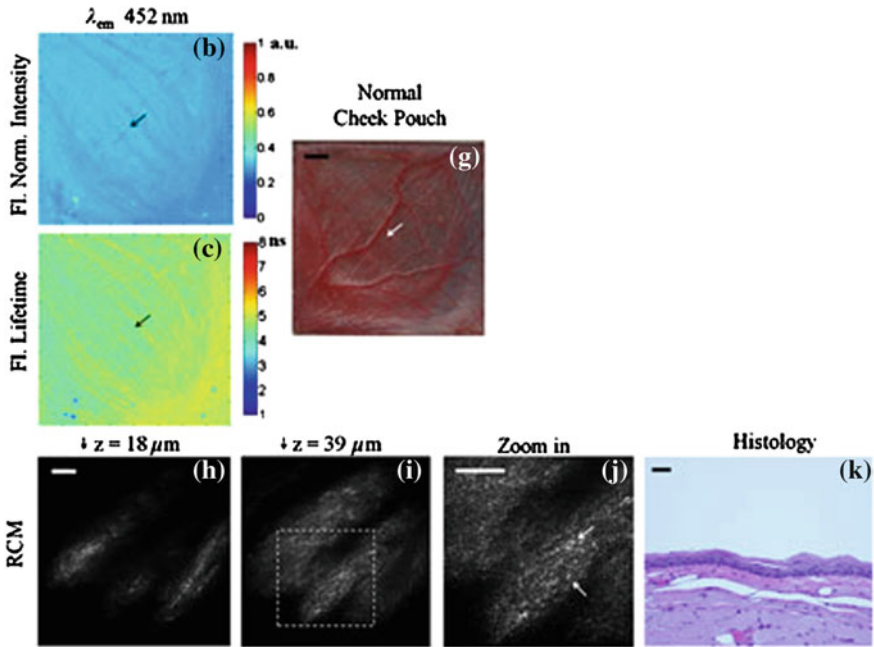


Fig. 14.10 **b, c** FLIM images of normal hamster cheek pouch at the NAD(P)H emission band (normalized intensity and lifetime). **g** Photograph of FLIM imaging area. *Arrows* indicate RCM imaging region. **h–i** RCM images taken at indicated depths. **j** Zoomed in image taken from dotted square in **(i)**. *White arrows* indicate nuclei. **k** H&E histology image from RCM region. *Scale bars* **a** and **g** 2 mm, and **h, j,** and **k** 50 μm . Reproduced with permission from [30]

for up to 8 h can represent *in vivo* metabolic states [50, 61]. Walsh et al. compared the NAD(P)H lifetime in hamster cheek epithelia *in vivo*, in live cultured biopsies up to 48 h, and in flash-frozen and thawed samples [59]. The mean lifetime of NAD(P)H in cultured tissue appears to have a lifetime similar to that of *in vivo* tissue through 4 h, while the frozen-thawed sample is 13 % greater, a significant difference ($p < 0.001$). By 12 h, the mean lifetime of NAD(P)H decreases significantly by 10 % and remains significantly lower than the *in vivo* value (Fig. 14.12).

These measurements suggest that optical metabolism measurements from tissue that has been cultured for up to 8 h represent the metabolic state of the *in vivo* tissue. The metabolic state of frozen-thawed tissue does not represent that of *in vivo* tissue. Cells undergoing stress, such as apoptosis, have also shown increased mean NAD(P)H fluorescence lifetimes, suggesting that freezing and thawing tissue exerts more stress on cells than live culture [61]. While optical metabolic measurements varied from *in vivo* values after 8 h of live culture, cell morphology and histological analysis did not show any changes over the entire time course of the experiment. This suggests that NAD(P)H lifetime measurements are more sensitive to molecular changes than these standard analysis methods.

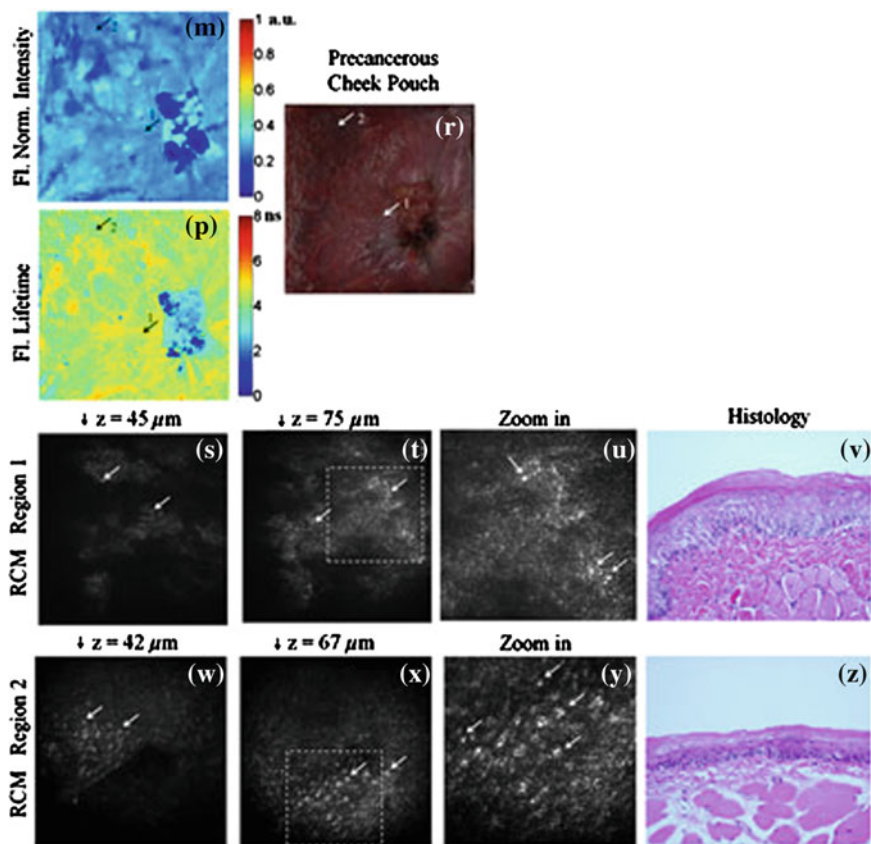


Fig. 14.11 **m, p** FLIM images of DMBA-treated hamster cheek pouch at the NAD(P)H emission band (normalized intensity and lifetime). **r** Photograph of FLIM imaging area. *Arrows* indicate RCM imaging regions (**s–t, w–x**) RCM images taken at indicated depths and regions. **u, y** Zoomed in images taken from *dotted square* in (**t, x**). *White arrows* indicate nuclei. **v, z** H&E histology image from RCM region. Scale same as Fig. 14.10. Reproduced with permission from [30]

Conklin et al. demonstrated that fluorescence measurements of endogenous NAD(P)H can be made accurately in fixed tissue samples such as classic histopathology slides [6]. Histology allows a pathologist to identify morphological changes that provide a high degree of accuracy in tumor staging and prediction of patient outcome. The authors demonstrate that mouse mammary tumors can be distinguished from normal epithelium by multiphoton FLIM measurements in unstained histopathology slides, allowing detection of changes in the metabolic state of tumor cells. Staining with hematoxylin and eosin (H&E) was shown to interfere with endogenous fluorescence measurements. The mice in this study were transgenic for the polyomavirus middle-T (PyVMT) oncogene under the control of the mammary specific MMTV promoter to generate primary tumors. This breast tumor model reliably demonstrates the progression from hyperplasia to adenoma to

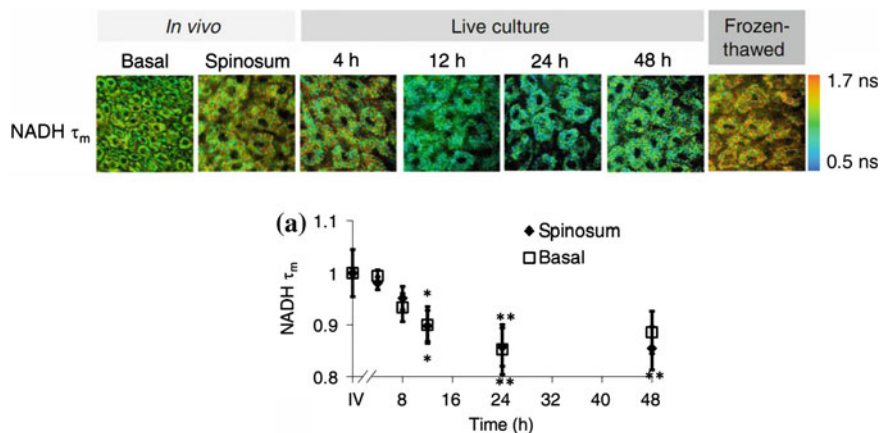


Fig. 14.12 *Top* Representative NAD(P)H τ_m images from each location and time point. *Bottom* NAD(P)H τ_m relative to in vivo value (* $p < 0.05$; ** $p < 0.01$). Reproduced with permission from [59]

Table 14.1 Components of NAD(P)H fluorescence lifetime in tumor epithelium versus normal epithelium

	τ_1 (ps)		τ_2 (ps)		a_1	
	Normal	Tumor	Normal	Tumor	Normal	Tumor
780 nm excitation	456	546	2360	2538	47	49
Average shift	(90)		(178)		(2)	
[$n = 10$]	*					

Reproduced with permission from [19]

* denotes that the tumor value is significant compared to the normal value, $p < 0.05$ for a Student's t-test

carcinoma in a manner closely resembling human ductal carcinoma in situ, and is dependably invasive and metastatic [43].

The study focused on the carcinoma in situ (CIS) stage of disease progress, which is similar to human ductal carcinoma in situ (DCIS), and is of interest for seeking optical biomarkers of cancer because it contains normal epithelium contiguous with tumor neoplasia. A mouse mammary tumor was sectioned and imaged unstained with both normal and tumor epithelium visible. The short component of NAD(P)H lifetime was found to undergo a statistically significant increase in tumor epithelium versus normal tissue (Table 14.1). Finally, the section was stained with H&E to show the ability to subsequently investigate cell morphology.

This data suggests that combining fluorescence imaging of unstained slides with subsequent classic bright-field imaging of H&E stains can give a more advanced diagnosis of disease state than either alone. Surprisingly, endogenous fluorescence of cells is preserved throughout histological processes including fixing, sectioning, and de-paraffinizing.

Preclinical models of human cancers and other disease states are invaluable in the development and testing of new devices that measure the fluorescence lifetime of NAD(P)H in tissues both *in vivo* and *ex vivo*. Despite imperfections in the ability of these models to accurately represent genetically and phenotypically heterogeneous human diseases, their use will continue to be an important step in the translation of NAD(P)H lifetime technologies to the clinical setting.

14.4 Clinical Applications

Due to the promising results obtained in cells and tissues, time-resolved fluorescence imaging and spectroscopy has the potential for a multitude of clinical applications. These applications necessarily include also other endogenous fluorophores, such as FAD, lipofuscin, melanin, and porphyrins [17, 22, 35, 52, 53]. Clinical instruments are on the market for ophthalmology [23, 52–54] and dermatology [36, 37], see Chaps. 15 and 16 of this book.

Current efforts of NAD(P)H FLIM translation are predominately in accessible tissues—the skin, and the oral cavity [9, 10, 45]; however, studies of biopsied tissues include also interrogation of brain, colon, and breast tissues [13, 20, 25, 43, 62]. Clinically, time resolved NAD(P)H fluorescence endpoints are used to differentiate normal from malignant and pre-malignant tissues, and identify tumor margins.

Early experiments of time-resolved NAD(P)H fluorescence were performed with single-point spectroscopy measurements on excised tissues. The NAD(P)H fluorescence lifetime of excised tissues recapitulates the *in vivo* state as long as the tissue is hydrated and imaged within several hours [50, 59]. De Beule et al. used a hyperspectral fluorescence lifetime probe for skin cancer diagnosis [20]. This system used two picosecond lasers emitting light at 355 and 440 nm and collected spectrally resolved fluorescence emission between 390 and 600 nm. This system utilized multi-wavelength TCSPC [4–6] at 16 emission channels in combination with laser multiplexing [4–6] (see Chap. 1, Sects. 1.4.1 and 1.4.2) to simultaneously obtain spectrally resolved lifetime data at two excitation wavelengths. De Beule et al. found no significant difference between the fluorescence lifetimes of basal cell carcinoma and normal, surrounding tissue when excited with 355 nm light [20]. However, it is important to note that the point measurement provides an average value over the probed area and the fluorescence signal from the tissue excited at 355 nm may include fluorescence emission from not only NAD(P)H, but also collagen, keratin and melanin. Significant improvement was obtained by single-point multi-wavelength TCSPC in a micro-spectrometric setup [14–16], see Chap. 13.

However, for clinical use fluorescence lifetime detection must be combined with imaging and, if possible, with spectrally resolved detection. Acquisition times should be in the range of a few seconds or below, the data should be recorded in a sufficiently large number of time channels to resolve double-exponential decay function into their components, and the laser power should be within the limits of laser safety standards.

Cheng et al. designed a FLIM system with a rigid probe of diameter 1.7 cm and a length of 14 cm [12]. Imaging was performed by scanning, time-resolved recording by using analog-signal detection and recording by a fast digitizer. A frequency-tripled Nd:YAG laser with excitation wavelength 355 nm and 1 ns pulse length was used for excitation. Images of 150×150 pixels were obtained within an acquisition time of 1 s. The endoscope was tested in vivo in healthy epithelium of a hamster cheek pouch model, and spatially uniform NAD(P)H autofluorescence lifetime data was measured as expected (Fig. 14.13, left). The time resolution of the detection system was 320 ps, deconvolution of the impulse response function was performed offline using an optimized Laguerre algorithm (CITE). It delivered a mean NAD(P)H lifetime of 4.44 ± 0.13 ns. This accuracy was considered sufficient for clinical imaging of oral cancer.

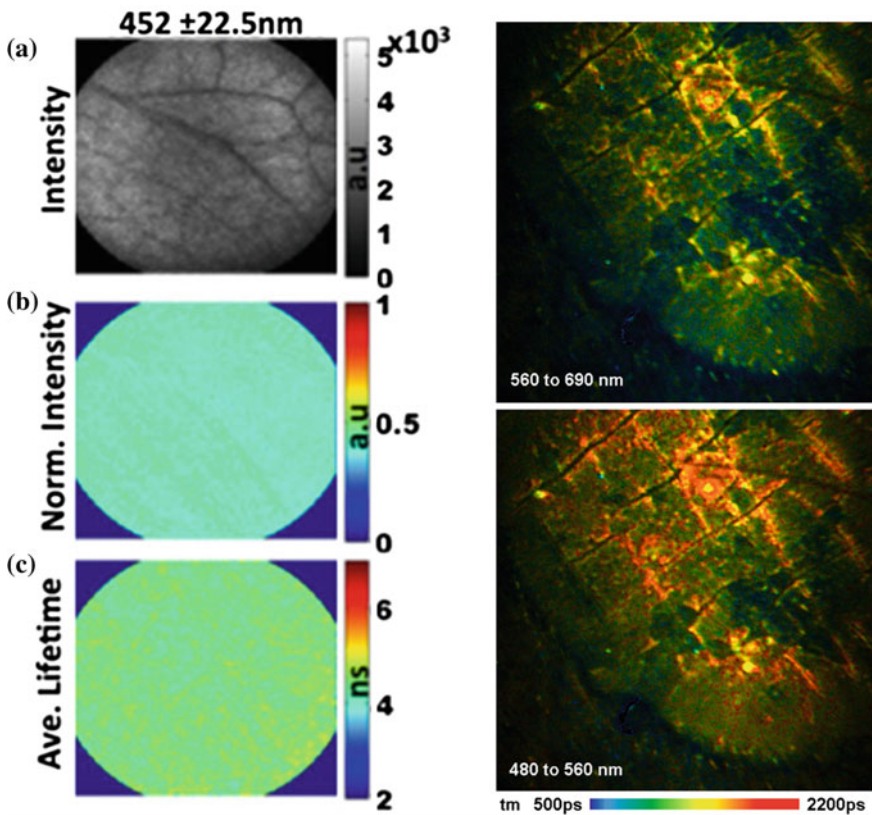


Fig. 14.13 Endoscope testing in vivo. *Left* Images obtained by Cheng et al. Maps of NAD(P)H (452 ± 22.5 nm emission). **a** Absolute intensity, **b** normalized intensity, and **c** average lifetime. 150×150 pixels, acquisition time 1 s. Reproduced with permission from [12]. *Right* Image obtained by TCSPC FLIM and scanning through an endoscope, see Chap. 2, Sect. 2.6. Keratome on human skin, 512×512 pixels, two wavelength channels, image area 5×5 mm, acquisition time 20 s

The advantage of this device is that it can achieve relatively high imaging speed without loss of temporal resolution. The sampling rate of the digitiser (one sample per 150 ps) allows for deconvolution of the non-ideal instrument response for accurate single-exponential lifetime analysis but not necessarily for double exponential analysis. The disadvantage is that the photon efficiency of analog recording is lower than for photon counting, and high excitation power is used. It should also be noted that the acquisition time of 1 s was obtained at a relative moderate number of pixels. For images of the same pixel number TCSPC FLIM is not significantly slower [6, 32].

The FLIM technique with the highest temporal resolution and with the highest photon efficiency is TCSPC FLIM. The principle is described in Chap. 1 of this book, the combination with optical imaging techniques in Chap. 2. For clinical imaging, TCSPC FLIM is often considered too slow in terms of acquisition time. This is not necessarily correct, as has been shown in [4, 5, 33]: Acquisition times on the order of one second can be achieved, see also Chap. 2, Sect. 2.2.4. TCSPC FLIM can be combined with multi-spectral detection [4–6], see Chap. 1, Sect. 1.4.5.2. Multi-spectral TCSPC FLIM in combination with a two-photon laser scanning microscope has been introduced [3] and the applicability to NAD(P)H detection been demonstrated by Becker et al. [4–6] and Rück et al. [48]. The technique has been used for NAD(P)H imaging [63], for identification of malignant melanoma in skin [22], and for diagnosis of squamous intraepithelial neoplasia [39]. A system with 8 fully parallel spectral channels working at an acquisition time of 5 s has been described in [6].

TCSPC FLIM systems are available not only for microscopy but also imaging of cm-sized objects. These are placed directly in the primary image plane of a confocal scanner [6], see Chap. 2, Sect. 2.5. Scanning has also been demonstrated through flexible [33] endoscopes. TCSPC FLIM by scanning through a rigid endoscope is described in Chap. 2, Sect. 2.6 of this book. The system delivered excellent spatial and temporal resolution and an acquisition time of 10–20 s for images of 512×512 pixels. The acquisition time can probably be reduced by a factor 16 for images of 128×128 pixels. Images obtained with this system is shown in Fig. 14.13, right.

14.4.1 *Ex Vivo Tissue Studies*

Time-resolved NAD(P)H fluorescence spectroscopy and imaging has been explored in a variety of tissues, including skin, brain, breast, head and neck tissues, and colon. However, it is often difficult to separate NAD(P)H autofluorescence from that of other endogenous fluorophores including collagen, keratin, and FAD in tissues. The NAD(P)H fluorescence signal can be separated from collagen and FAD by spectrally resolved emission data and the fluorescence lifetime [38, 40, 41, 63]. Collagen has a

much longer lifetime ($\sim 5\text{--}6$ ns) than NAD(P)H, and emission is typically at shorter wavelengths than NAD(P)H emission [41]. Many of the studies discussed herein excite tissue at a single wavelength and collect wave-length resolved emission spectrum to infer trends across samples for different fluorophores. NAD(P)H can be excited in the 330–400 nm range (660–800 nm two-photon) and emission is centred around 450 nm [29, 41].

While the probe-based single-point spectroscopy study of Kennedy et al. [33] did not find significant differences in the lifetime between basal cell carcinoma and normal tissue, an imaging study was able to delineate between the two tissue states. In a subsequent study, Galletly et al. used a wide-field macroscopic time-domain FLIM system to interrogate basal cell carcinoma and normal tissue [25]. This system excited tissue at 355 nm and collected emission at either 375 or 455 nm, with the assumption that the fluorescence signal collected at 375 nm is predominately from collagen while the emission from 455 nm is predominately from NAD(P)H. Fluorescence lifetime data was acquired using a CCD camera with a gated optical intensifier to obtain 25 time gates at 250 ps intervals. Galletly et al. report a significantly ($p < 0.0001$) reduced mean fluorescence lifetime (1.402 ± 0.127 ns basal cell carcinoma versus 1.554 ± 0.141 ns normal) of basal cell carcinomas in the 455 nm emission channel [25]. Due to this difference in fluorescence lifetimes, FLIM shows promise for in vivo detection and diagnosis of basal cell carcinoma. In addition to basal cell carcinoma, time-resolved fluorescence imaging has been investigated for melanoma detection and diagnosis. In a study by Dimitrow et al., fluorescence lifetime images of skin lesions were acquired both in vivo and from biopsies [22]. This study reports decreased short and long lifetime values with two-photon excitation at 760 nm in melanocytes compared to normal tissue but no lifetime changes in melanoma.

Time resolved fluorescence imaging of human tissue NAD(P)H is not limited to skin, but has also been performed on biopsies of colon, stomach, bladder, liver and pancreas. In this study by McGinty et al., a wide-field fluorescence lifetime imaging system detected fluorescence lifetime data by a gated optical intensifier coupled to a CCD camera which recorded images at 25 different time points with 250 ps intervals [44]. The tissue was excited at 355 nm and emission was collected with a 375 nm long-pass filter. McGinty et al. found that the fluorescence lifetime of colon tumors increased compared to normal colon tissue [44]. Additionally, they observed increased (but not statistically significant) fluorescence lifetimes of gastric cancer and bladder cancer [44]. Two precancerous colon lesions exhibited decreased mean fluorescence lifetimes [44]. Due to the 355 nm excitation and 375 nm long-pass filter, most of the fluorescence signal was most likely from NAD(P)H, however, there may be a contribution from collagen and/or keratin in this study. Additionally, McGinty et al. demonstrated an imaging system utilizing only two time gates to build a fluorescence decay curve which was capable of video rate (10 Hz) acquisition speeds, which provides real-time imaging for point-of-care or intraoperative use [44].

In addition to these abdominal cancers, NAD(P)H FLIM has been performed on slices of human brain biopsies. In the brain, multiphoton excited NAD(P)H fluorescence lifetimes are often fit to three lifetimes due to an additional long lifetime often attributed to an additional bound species [13]. In *ex vivo* measurements from brain glioma tissue samples, a spectroscopic time-resolved fluorescence probe excited tissue at 337 nm and a 460 nm bandpass filter isolated NAD(P)H emission [62]. The lifetime of 460 nm emission was shortest in cerebral cortex (1.1 ns), slightly greater in low grade glioma (1.15 ns), greater in high grade glioma (1.3 ns), and greatest in normal white matter (1.8 ns) [62]. While the lifetime at 460 nm alone was not sufficient to classify tissue as benign or malignant, additional information including the lifetime at 390 nm (collagen) and fluorescence intensities resulted in a classification algorithm with an accuracy above 90 % [62].

Kantelhardt et al. [31] and Leppert et al. [42] used two-photon excitation and TCSPC FLIM to record lifetime images of glioma and the surrounding brain tissue. They found a significantly increased mean (amplitude-weighted) lifetime for the glioma cells compared to the surrounding brain cells.

14.4.2 *In Vivo Human Studies*

In addition to investigating excised human tissues, time-resolved fluorescence imaging of NAD(P)H has been performed *in vivo* for diagnosis and margin assessment of brain and head and neck cancers. In the brain, time-resolved fluorescence spectroscopy measurements have identified longer NAD(P)H lifetimes in low grade glioma ($\tau = 1.38$ ns) than normal white matter ($\tau = 1.19$ ns), normal cortex ($\tau = 1.16$ ns) and high grade glioma ($\tau = 1.13$ ns) [9, 10]. Using the spectral and lifetime characteristics of NAD(P)H and collagen, this study classified low grade gliomas with 100 % sensitivity and 94 % specificity [10].

In head and neck cancers, time-resolved measurements of NAD(P)H fluorescence are explored as a means of diagnosing cancerous tissue. A non-invasive diagnostic tool is particularly important for head and neck cancers to preserve tissue and function of vital organs—such as the tongue, mouth, esophagus, and vocal box. When head and neck squamous cell carcinomas are excited at 337 nm and the emission at 460/25 nm collected, the lifetime of cancerous tissue is significantly shorter than normal tissue [45, 58]. A wide-field FLIM system with a 4 mm field of view quickly collects and graphically displays NAD(P)H lifetimes for intraoperative margin assessment [58]. Representative images are shown in Fig. 14.14, demonstrating the added contrast of the lifetime measurements over fluorescence intensity or bright field imaging alone [58].

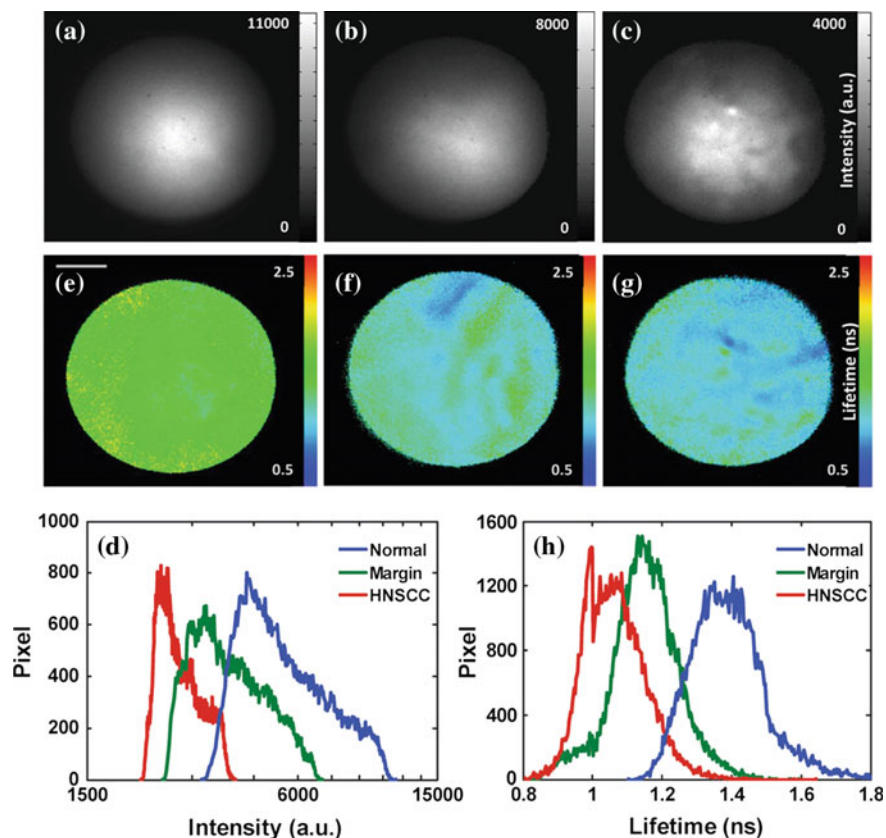


Fig. 14.14 Autofluorescence fluorescence lifetime imaging microscopy images of human buccal mucosa: (a–c) depict the intensity images, and (e–g) depict the average lifetime images from three areas: normal, tumor, and adjacent normal-tumor, their corresponding histograms are depicted in (d) for intensity and (h) for average lifetime. HNSCC, head and neck squamous cell carcinoma. Reproduced with permission from [58]

14.5 Conclusions

Fluorescence lifetime imaging of NAD(P)H provides specific information on the relative amounts of free and protein-bound NAD(P)H in a cell. This unique metabolic endpoint has been characterized with controlled experiments in cell culture, and has been applied to understand disease progression in animal models. Due to the non-invasive nature of these measurements, NAD(P)H fluorescence lifetime imaging has also been used to characterize human tissue *in vivo*, and several *ex vivo* human tissue studies also hold promise for future translation, see Chaps. 2, 13, 14–16. Recent technological developments have improved the acquisition time of fluorescence lifetime imaging techniques. TCSPC FLIM with laser scanning has been shown to

record lifetime images at acquisition times of less than one second [32], and spectrally resolved lifetime images within 5 s [6]. Dynamic effects in the fluorescence lifetime of a sample can be recorded at a resolution of 1 ms by line scanning TCSPC [8], and at a resolution of 40 ms by temporal mosaic FLIM, see Chaps. 2 and 5 of this book. TCSPC FLIM can be performed in image areas in the cm² range, and through optical periscopes, see Chap. 2. Motion artefacts can be eliminated by parallel IR imaging and aligning subsequent frames online (see Chap. 16), probably also by recording individual frames by mosaic FLIM and aligning the frames on-line or off-line. Wide-field FLIM techniques by gated camera have been improved to record images in several time windows simultaneously, thus increasing the photon efficiency and reducing the acquisition time [21, 24, 26, 47, 58]. Thus, there is a wide range of technologies capable of capturing the relatively weak signals of NAD(P)H and using them for clinical applications.

References

1. S. Andrejevic, J.F. Savary, C. Fontolliet, P. Monnier, H. van Den Bergh, 7,12-dimethylbenz[a]anthracene-induced ‘early’ squamous cell carcinoma in the Golden Syrian hamster: evaluation of an animal model and comparison with ‘early’ forms of human squamous cell carcinoma in the upper aero-digestive tract. *Int. J. Exp. Pathol.* **77**, 7–14 (1996)
2. S. Banerjee, D.K. Bhatt, Histochemical studies on the distribution of certain dehydrogenases in squamous cell carcinoma of cheek. *Indian J. Cancer* **26**, 21–30 (1989)
3. W. Becker, A. Bergmann, C. Biskup, T. Zimmer, N. Klöcker, K. Benndorf, Multi-wavelength TCSPC lifetime imaging. *Proc. SPIE* **4620**, 79–84 (2002)
4. W. Becker, *Advanced Time-Correlated Single-Photon Counting Techniques* (Springer, Berlin, 2005)
5. W. Becker, A. Bergmann, C. Biskup, Multi-spectral fluorescence lifetime imaging by TCSPC. *Microsc. Res. Technol.* **70**, 403–409 (2007)
6. W. Becker, *The bh TCSPC Handbook*, 5th edn. (Becker & Hickl GmbH 2012). www.becker-hickl.com
7. W. Becker, V. Shcheslavkiy, S. Frere, I. Slutsky, Spatially resolved recording of transient fluorescence-lifetime effects by line-scanning TCSPC. *Microsc. Res. Technol.* **77**, 216–224 (2014)
8. D.K. Bird, L. Yan, K.M. Vrotsos, K.W. Eliceiri, E.M. Vaughan, P.J. Keely, J.G. White, N. Ramanujam, Metabolic mapping of MCF10A human breast cells via multiphoton fluorescence lifetime imaging of the coenzyme NADH. *Cancer Res.* **65**, 8766–8773 (2005)
9. P.V. Butte, Q. Fang, J.A. Jo, W.H. Yong, B.K. Pikul, K.L. Black, L. Marcu, Intraoperative delineation of primary brain tumors using time-resolved fluorescence spectroscopy. *J. Biomed. Opt.* **15**, 027008 (2010)
10. P.V. Butte, A.N. Mamelak, M. Nuno, S.I. Bannykh, K.L. Black, and L. Marcu, Fluorescence lifetime spectroscopy for guided therapy of brain tumors. *NeuroImage* **54** (Suppl 1), S125–135 (2011)
11. B. Chance, B. Schoener, R. Oshino, F. Itshak, Y. Nakase, Oxidation-reduction ratio studies of mitochondria in freeze-trapped samples. NADH and flavoprotein fluorescence signals. *J. Biol. Chem.* **254**, 4764–4771 (1979)
12. S. Cheng, R.M. Cuenca, B. Liu, B.H. Malik, J.M. Jabbour, K.C. Maitland, J. Wright, Y.S. Cheng, J.A. Jo, Handheld multispectral fluorescence lifetime imaging system for in vivo applications. *Biomed. Opt. Express* **5**, 921–931 (2014)

13. T.H. Chia, A. Williamson, D.D. Spencer, M.J. Levene, Multiphoton fluorescence lifetime imaging of intrinsic fluorescence in human and rat brain tissue reveals spatially distinct NADH binding. *Opt. Express* **16**, 4237–4249 (2008)
14. A. Chorvat, Chorvatova, Spectrally resolved time-correlated single photon counting: a novel approach for characterization of endogenous fluorescence in isolated cardiac myocytes. *Eur. Biophys. J.* **36**, 73–83 (2006)
15. D. Chorvat, A. Chorvatova, Multi-wavelength fluorescence lifetime spectroscopy: a new approach to the study of endogenous fluorescence in living cells and tissues. *Laser Phys. Lett.* **6**, 175–193 (2009)
16. D. Chorvat Jr., A. Mateasik, Y.G. Cheng, N.Y. Poirier, J. Miro, N.S. Dahdah, A. Chorvatova, Rejection of transplanted hearts in patients evaluated by the component analysis of multi-wavelength NAD(P)H fluorescence lifetime spectroscopy. *J. Biophotonics.* **3** 646–652 (2010)
17. A. Chorvatova, D. Chorvat, Tissue fluorophores and their spectroscopic characteristics, in *Fluorescence Lifetime Spectroscopy and Imaging*, ed. by L. Marcu, P.W.M. French, D.S. Elson (CRC Press, Boca Raton, 2015)
18. A.L. Clark, A. Gillenwater, R. Alizadeh-Naderi, A.K. El-Naggar, R. Richards-Kortum, Detection and diagnosis of oral neoplasia with an optical coherence microscope. *J. Biomed. Opt.* **9**, 1271–1280 (2004)
19. M.W. Conklin, P.P. Provenzano, K.W. Eliceiri, R. Sullivan, P.J. Keely, Fluorescence lifetime imaging of endogenous fluorophores in histopathology sections reveals differences between normal and tumor epithelium in carcinoma in situ of the breast. *Cell Biochem. Biophys.* **53**, 145–157 (2009)
20. P.A. De Beule, C. Dunsby, N.P. Galletly, G.W. Stamp, A.C. Chu, U. Anand, P. Anand, C.D. Benham, A. Naylor, P.M. French, A hyperspectral fluorescence lifetime probe for skin cancer diagnosis. *Rev. Scientific Instrum.* **78**, 123101 (2007)
21. P.A.B. De Beule, D.M. Owen, H.B. Manning, C.B. Talbot, J. Requejo-Isidro, C. Dunsby, J. McGinty, R.K.P. Benninger, D.S. Elson, I. Munro, M. John Lever, P. Anand, M.A.A. Neil, and P. M.W. French, Rapid hyperspectral fluorescence lifetime imaging. *Microsc. Res. Technol.* **70**, 481–484 (2007)
22. E. Dimitrow, I. Riemann, A. Ehlers, M.J. Koehler, J. Norgauer, P. Elsner, K. Konig, M. Kaatz, Spectral fluorescence lifetime detection and selective melanin imaging by multiphoton laser tomography for melanoma diagnosis. *Exp. Dermatol.* **18**, 509–515 (2009)
23. C. Dysli, G. Quelled, M. Abegg, M.N. Menke, U. Wolf-Schnurrbusch, J. Kowal, J. Blatz, O. La Schiazza, A.B. Leichtle, S. Wolf, M.S. Zinkernagel, Quantitative analysis of fluorescence lifetime measurements of the macula using the fluorescence lifetime imaging ophthalmoscope in healthy subjects. *IOVS.* **55**, 2107–2113 (2014)
24. D.S. Elson, I. Munro, J. Requejo-Isidro, J. McGinty, C. Dunsby, N. Galletly, G.W. Stamp, M. A.A. Neil, M.J. Lever, P.A. Kellett, A. Dymoke-Bradshaw, J. Hares, P.M.W. French, Real-time time-domain fluorescence lifetime imaging including single-shot acquisition with a segmented optical image intensifier. *New J. Phys.* **6**, 180 (2004)
25. N.P. Galletly, J. McGinty, C. Dunsby, F. Teixeira, J. Requejo-Isidro, I. Munro, D.S. Elson, M. A. Neil, A.C. Chu, P.M. French, G.W. Stamp, Fluorescence lifetime imaging distinguishes basal cell carcinoma from surrounding uninvolved skin. *Br. J Dermatol.* **159**, 152–161 (2008)
26. D.M. Grant, J. McGinty, E.J. McGhee, T.D. Bunney, D.M. Owen, C.B. Talbot, W. Zhang, S. Kumar, I. Munro, P.M. Lanigan, G.T. Kennedy, C. Dunsby, A.I. Magee, P. Courtney, M. Katan, M.A.A. Neil, P.M.W. French, High speed optically sectioned fluorescence lifetime imaging permits study of live cell signaling events. *Opt. Express* **15**, 15656–15673 (2007)
27. C.J. Gullledge, M.W. Dewhirst, Tumor oxygenation: a matter of supply and demand. *Anticancer Res.* **16**, 741–749 (1996)
28. H.W. Guo, C.T. Chen, Y.H. Wei, O.K. Lee, V. Gukassyan, F.J. Kao, H.W. Wang, Reduced nicotinamide adenine dinucleotide fluorescence lifetime separates human mesenchymal stem cells from differentiated progenies. *J. Biomed. Opt.* **13**, 050505 (2008)
29. S. Huang, A.A. Heikal, W.W. Webb, Two-photon fluorescence spectroscopy and microscopy of NAD(P)H and flavoprotein. *Biophys. J.* **82**, 2811–2825 (2002)

30. J.M. Jabbour, S. Cheng, B.H. Malik, R. Cuenca, J.A. Jo, J. Wright, Y.S. Cheng, K.C. Maitland, Fluorescence lifetime imaging and reflectance confocal microscopy for multiscale imaging of oral precancer. *J. Biomed. Opt.* **18**, 046012 (2013)
31. S.R. Kantelhardt, J. Leppert, J. Krajewski, N. Petkus, E. Reusche, V.M. Tronnier, G. Hüttmann, A. Giese, Imaging of brain and brain tumor specimens by time-resolved multiphoton excitation microscopy ex vivo. *Neuro-Onkology* **95**, 103–112 (2007)
32. V. Katsoulidou, A. Bergmann, W. Becker, How fast can TCSPC FLIM be made? *Proc. SPIE* **6771**, 67710B-1–67710B-7 (2007)
33. G.T. Kennedy, H.B. Manning, D.S. Elson, M.A.A. Neil, G.W. Stamp, B. Viellerobe, F. Lacombe, C. Dunsby, P.M.W. French, A fluorescence lifetime imaging scanning confocal endomicroscope. *J. Biophoton.* **3**, 103–107 (2010)
34. M. Köllner, J. Wolfrum, How many photons are necessary for fluorescence-lifetime measurements? *Phys. Chem. Lett.* **200**, 199–204 (1992)
35. K. König, I. Riemann, High-resolution multiphoton tomography of human skin with subcellular spatial resolution and picosecond time resolution. *J. Biomed. Opt.* **8**, 432–439 (2003)
36. K. König, Clinical multiphoton tomography. *J. Biophoton.* **1**, 13–23 (2008)
37. K. König, A. Uchugonova, in *FLIM Microscopy in Biology and Medicine*, ed. by A. Periasamy, R.M. Clegg. Multiphoton Fluorescence Lifetime Imaging at the Dawn of Clinical Application, (CRC Press, Boca Raton, 2009)
38. K. König, A. Uchugonova, E. Gorjup, Multiphoton fluorescence lifetime imaging of 3d-stem cell spheroids during differentiation. *Microsc. Res. Techn.* **74**, 9–17 (2011)
39. S. Khoon Teh, W. Zheng, S. Li, D. Li, Y. Zeng, Y. Yang, J.Y. Qu, Multimodal nonlinear optical microscopy improves the accuracy of early diagnosis of squamous intraepithelial neoplasia. *J. Biomed. Opt.* **18**(3) 036001-1 to -11 (2013)
40. J.R. Lakowicz, H. Szmajnski, K. Nowaczyk, M.L. Johnson, Fluorescence lifetime imaging of free and protein-bound NADH. *Proc. Natl. Acad. Sci.* **89**, 1271–1275 (1992)
41. J. Lakowicz, *Principles of Fluorescence Spectroscopy*, 3rd edn. (Springer, Berlin, 2006)
42. J. Leppert, J. Krajewski, S.R. Kantelhardt, S. Schläffer, N. Petkus, E. Reusche, G. Hüttmann, A. Giese, Multiphoton excitation of autofluorescence for microscopy of glioma tissue. *Neurosurgery* **58**, 759–767 (2006)
43. E.Y. Lin, J.G. Jones, P. Li, L. Zhu, K.D. Whitney, W.J. Muller, J.W. Pollard, Progression to malignancy in the polyoma middle T oncoprotein mouse breast cancer model provides a reliable model for human diseases. *Am. J. Pathol.* **163**, 2113–2126 (2003)
44. J. McGinty, N.P. Galletly, C. Dunsby, I. Munro, D.S. Elson, J. Requejo-Isidro, P. Cohen, R. Ahmad, A. Forsyth, A.V. Thillainayagam, M.A. Neil, P.M. French, G.W. Stamp, Wide-field fluorescence lifetime imaging of cancer. *Biomed. Opt. Express* **1**, 627–640 (2010)
45. J.D. Meier, H. Xie, Y. Sun, Y. Sun, N. Hatami, B. Poirier, L. Marcu, D.G. Farwell, Time-resolved laser-induced fluorescence spectroscopy as a diagnostic instrument in head and neck carcinoma, Otolaryngology–head and neck surgery. *Am. J. Otolaryngol Head Neck Surg.* **142**, 838–844 (2010)
46. N. Ramanujam, Fluorescence spectroscopy of neoplastic and non-neoplastic tissues. *Neoplasia* **2**, 89–117 (2000)
47. J. Requejo-Isidro, J. McGinty, I. Munro, D.S. Elson, N.P. Galletly, M.J. Lever, M.A.A. Neil, G.W.H. Stamp, P.M.W. French, P.A. Kellett, J.D. Hares, A.K.L. Dymoke-Bradshaw, High-speed wide-field time-gated endoscopic fluorescence-lifetime imaging. *Opt. Lett.* **29**, 2249–2251 (2004)
48. A. Rück, Ch. Hülshoff, I. Kinzler, W. Becker, R. Steiner, SLIM: a new method for molecular imaging. *Microsc. Res. Technol.* **70**, 403–409 (2007)
49. B.A. Ruggeri, F. Camp, S. Miknyoczki, Animal models of disease: pre-clinical animal models of cancer and their applications and utility in drug discovery. *Biochem. Pharmacol.* **87**, 150–161 (2014)

50. W.Y. Sanchez, T.W. Prow, W.H. Sanchez, J.E. Grice, M.S. Roberts, Analysis of the metabolic deterioration of ex-vivo skin, from ischemic necrosis, through the imaging of intracellular NAD(P)H by multiphoton tomography and fluorescence lifetime imaging microscopy (MPT-FLIM). *J. Biomed. Opt.* **15**(4), 046008 (2010)
51. H. Schneckenburger, M. Wagner, P. Weber, W.S. Strauss, R. Sailer, Autofluorescence lifetime imaging of cultivated cells using a UV picosecond laser diode. *J. Fluoresc.* **14**, 649–654 (2004)
52. D. Schweitzer, S. Schenke, M. Hammer, F. Schweitzer, S. Jentsch, E. Birckner, W. Becker, Towards metabolic mapping of the human retina. *Microsc. Res. Technol.* **70**, 403–409 (2007)
53. D. Schweitzer, in *Fundus Autofluorescence*, ed. by N. Lois, J.V. Forrester. Quantifying Fundus Autofluorescence. (Wolters Kluwer, Lippincott Williams & Wilkins, 2009)
54. D. Schweitzer, in *Metabolic Mapping* ed. by F.G. Holz, R.F. Spaide. Medical Retina Essential in Ophthalmology, (Springer, Berlin, 2010)
55. A.T. Shah, M. Demory Beckler, A.J. Walsh, W.P. Jones, P.R. Pohlmann, M.C. Skala, Optical metabolic imaging of treatment response in human head and neck squamous cell carcinoma. *PLoS ONE.* **9**, e90746 (2014)
56. M.C. Skala, K.M. Riching, D.K. Bird, A. Gendron-Fitzpatrick, J. Eickhoff, K.W. Eliceiri, P. J. Keely, N. Ramanujam, In vivo multiphoton fluorescence lifetime imaging of protein-bound and free nicotinamide adenine dinucleotide in normal and precancerous epithelia. *J. Biomed. Opt.* **12**, 024014 (2007)
57. M.C. Skala, K.M. Riching, A. Gendron-Fitzpatrick, J. Eickhoff, K.W. Eliceiri, J.G. White, N. Ramanujam, In vivo multiphoton microscopy of NADH and FAD redox states, fluorescence lifetimes, and cellular morphology in precancerous epithelia. *Proc. Natl. Acad. Sci. U.S.A.* **104**, 19494–19499 (2007)
58. Y. Sun, R. Liu, D.S. Elson, C.W. Hollars, J.A. Jo, J. Park, Y. Sun, L. Marcu, Simultaneous time- and wavelength-resolved fluorescence spectroscopy for near real-time tissue diagnosis. *Opt. Lett.* **33**, 630–632 (2008)
59. A.J. Walsh, K.M. Poole, C.L. Duvall, M.C. Skala, Ex vivo optical metabolic measurements from cultured tissue reflect in vivo tissue status. *J. Biomed. Opt.* **17**, 116015 (2012)
60. A.J. Walsh, R.S. Cook, H.C. Manning, D.J. Hicks, A. Lafontant, C.L. Arteaga, M.C. Skala, Optical metabolic imaging identifies glycolytic levels, subtypes, and early-treatment response in breast cancer. *Cancer Res.* **73**, 6164–6174 (2013)
61. H.W. Wang, V. Gukassyan, C.T. Chen, Y.H. Wei, H.W. Guo, J.S. Yu, F.J. Kao, Differentiation of apoptosis from necrosis by dynamic changes of reduced nicotinamide adenine dinucleotide fluorescence lifetime in live cells. *J. Biomed. Opt.* **13**, 054011 (2008)
62. W.H. Yong, P.V. Butte, B.K. Pikul, J.A. Jo, Q. Fang, T. Papaioannou, K. Black, L. Marcu, Distinction of brain tissue, low grade and high grade glioma with time-resolved fluorescence spectroscopy. *Frontiers in bioscience : a journal and virtual library* **11**, 1255–1263 (2006)
63. Y. Zeng, B. Yan, Q. Sun, S. Khoon Teh, W. Zhang, Z. Wen, Jianan Y. Qu, Label-free in vivo imaging of human leukocytes using two-photon excited endogenous fluorescence. *J. Biomed. Opt.* **18**(4), 040103-1–040103-3 (2013)